


Article

Effect of Wall Thickness and Surface Conditions on Creep Behavior of a Single-Crystal Ni-Based Superalloy

Selina Körber ¹, Silas Wolff-Goodrich ², Rainer Völkl ¹ and Uwe Glatzel ^{1,*} 

¹ Metals and Alloys, University of Bayreuth, Prof.-Rüdiger-Bormann-Str. 1, 95447 Bayreuth, Germany; selina.koerber@uni-bayreuth.de (S.K.); rainer.voelkl@uni-bayreuth.de (R.V.)

² Max-Planck-Institut für Eisenforschung GmbH, Max-Planck-Str. 1, 40237 Duesseldorf, Germany; swolffgoodrich@gmail.com

* Correspondence: uwe.glatzel@uni-bayreuth.de; Tel.: +49-921-55-6600

Abstract: The influence of wall thickness and specimen surface on the creep behavior of the single-crystal nickel-based superalloy MAR M247LC is studied. Specimens with wall thicknesses of 0.4, 0.8, 1 and 2 mm, with and without casting surface, are compared to specimens of the same wall thickness prepared from bulk material. Creep behavior turned out to be independent from surface conditions even for the thinnest specimens. The thickness debit effect is not pronounced for short creep rupture times (≤ 100 h at 980 °C), whereas it is significant for creep rupture times longer than ~ 200 h at 980 °C. The thickness debit effect is time-dependent and caused by oxidation and diffusion-controlled mechanisms.

Keywords: creep; thin-walled; casting surface; single crystal; MAR M247LC



Citation: Körber, S.; Wolff-Goodrich, S.; Völkl, R.; Glatzel, U. Effect of Wall Thickness and Surface Conditions on Creep Behavior of a Single-Crystal Ni-Based Superalloy. *Metals* **2022**, *12*, 1081. <https://doi.org/10.3390/met12071081>

Academic Editor: Marcello Cabibbo

Received: 21 April 2022

Accepted: 20 June 2022

Published: 24 June 2022

Publisher's Note: MDPI stays neutral with regard to jurisdictional claims in published maps and institutional affiliations.



Copyright: © 2022 by the authors. Licensee MDPI, Basel, Switzerland. This article is an open access article distributed under the terms and conditions of the Creative Commons Attribution (CC BY) license (<https://creativecommons.org/licenses/by/4.0/>).

1. Introduction

Decreasing wall thicknesses and ever filigree partitioning walls in turbine blades promise better aerodynamics, higher cooling efficiencies and weight savings. However, previous investigations have shown that creep properties may deteriorate with decreasing wall thicknesses. This so-called thickness debit effect can affect the service life of turbine components.

Gibbons [1] gives an overview of the influence of specimen thickness on the relative service life of different conventionally cast (CC) and directionally solidified (DS) nickel-based superalloys. A comparison by Duhl [2] between conventionally cast (CC), directionally solidified (DS) and single crystal (SX) nickel-based superalloys shows that wall thicknesses below 4.0 mm lead to a strong deterioration in creep properties. The thickness debit effect is less pronounced in directionally solidified (DS/SX) specimens than in conventionally cast polycrystalline (CC) specimens [2]. In the case of polycrystalline and directionally solidified specimens, the grain size and morphology play important roles, since failure is mainly caused by crack formation at grain boundaries [3–7]. Furthermore, casting defects such as pores lead to a deterioration in creep properties, since these significantly reduce the load-bearing cross-section in thin-walled specimens [4,6,7].

Pandey et al. [8,9] compare creep behavior of round and hollow specimens of the nickel-based superalloy IN X750 and show that the service life of hollow specimens is significantly lower than that of round specimens. A critical wall thickness of 3.2 mm is defined for round specimens and 2.0 mm for hollow specimens [8,9]. Doner and Heckler [3,6] illustrate that 0.5 mm thin flat samples of the nickel-based superalloy CMSX-3 show significantly shorter life times than round specimens with a diameter of 6.4 mm.

Seetharaman and Cetel [10] study the creep behavior of the single-crystal nickel-based superalloy PWA1484. They show that reducing the wall thickness from 1.0 to 0.3 mm leads to a reduction in the fracture time to 30%. A pronounced thickness debit effect is observed in strong alumina-forming nickel-based superalloys due to the formation of γ' -depleted or γ' -free regions, respectively [11–17].

The presented literature generally reports results from creep tests on specimens having a much smaller size in one cross-sectional dimension than in the perpendicular dimension. The term “thickness”, how it is used here, means the size in the smaller dimension in mm. Thus, differences in creep behavior are inherently attributed to cross-sectional areas. A question to be answered, therefore, is at what thickness does the cross-sectional area become a critical factor determining the creep properties.

Previous investigations were almost exclusively carried out on thin-walled specimens that were prepared from bulk material [13,16,17]. The focus of this work is the creep behavior of “thin-cast” nickel-based superalloy MAR M247LC single-crystals, with single-crystals having wall thicknesses down to 0.4 mm. In addition, the influence of the specimen surface on creep properties is investigated.

2. Materials and Methods

2.1. Material

Thin-walled single-crystals of the nickel-based superalloy MAR M247LC were cast via Bridgman process in an induction furnace under vacuum at a pressure of 0.1 Pa. The composition of MAR M247LC is given in Table 1.

Table 1. Composition of MAR M247LC in wt.%.

Ni	Cr	Co	Mo	W	Al	Ti	Ta	Hf	C	B	Zr
61.5	8.1	9.3	0.5	9.4	5.7	0.7	3.3	1.4	0.07	0.017	0.007

Batches of the master alloy were placed in a ceramic crucible and hereafter induction melted. The molten material was poured into a ceramic mold that was preheated to a temperature of 1450 °C and positioned on a water-cooled Cu plate. After that, the ceramic shell mold was withdrawn through a water-cooled Cu baffle with a rate of 3 mm/min, as described in the work of Konrad et al. [18]. The ceramic shell molds for thin-walled casting were applied on 3D-printed positive polymer models instead of conventional wax models manufactured via injection molding [19].

Thin-walled single-crystal specimens with wall thicknesses of 0.4, 0.8, 1.0 and 2.0 mm were cast. Detailed investigations of the as-cast dendritic structure of these thin-cast specimens were already published [20]. Casting geometry is shown in Figure 1 and consisted of two thin-walled windows ($30 \times 8 \text{ mm}^2$), having wall thicknesses of 0.4, 0.8, 1.0 or 2.0 mm, respectively.

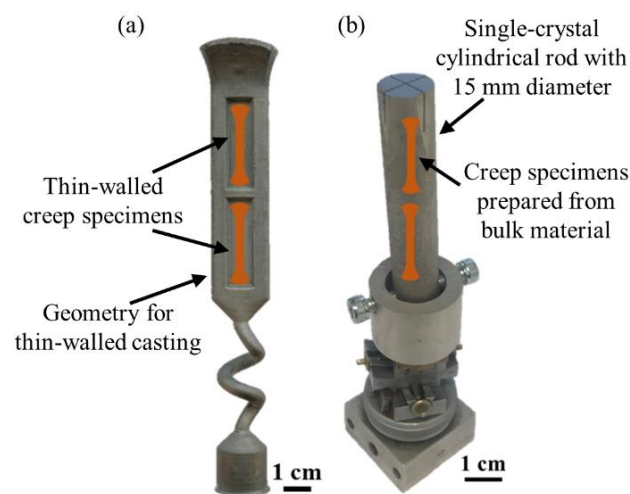


Figure 1. Casting geometry and schematic illustration of creep specimen preparation for (a) thin-walled castings and (b) single-crystal cylindrical rod.

Orientation of the single-crystal castings with respect to the [001] crystal direction was determined using electron backscattered diffraction (GeminiSEM Sigma VP 300, Zeiss, Jena, Germany). The deviation of the thin-walled castings was less than 5° in all cases. In addition, a cylindrical single crystal with a diameter of 15 mm and a length of 120 mm was cast for the preparation of thin creep specimens from bulk material. The cylindrical single crystal was oriented to the [001] direction within 2°.

All castings were subjected to a heat treatment under vacuum (10^{-3} – 10^{-4} Pa) consisting of a solution heat treatment at 1220, 1240 and 1250 °C for 2 h each. After cooling down to 1000 °C with cooling rates higher than 30 °C/min, a two-stage ageing was carried out at 1080 °C for 4 h and 900 °C for 8 h.

2.2. Creep Testing

Flat miniature creep specimens (overall length ~28.5 mm, gauge length ~4.00 mm; gauge width ~2.90 mm) were prepared from single-crystal castings using electrical discharge machining as schematically shown in Figure 1. For the here-called creep tests with casting surface, specimen surfaces were left untreated after heat treatment. For the here-called creep tests without casting surface, the specimen surface was ground with SiC paper with grits of 1000 after heat treatment. For the so-called creep tests on specimens prepared from bulk, the recast layer formed through electrical discharge machining on the heat-treated samples was removed by grinding with SiC paper.

The thickness of the gauge section of every individual miniature creep specimen was determined with a micrometer screw (precision ± 0.01 mm) and the width of the gauge section was determined with a caliper gauge (precision ± 0.01 mm), respectively.

For constant engineering stress creep tests, the load was applied to the sample through a steel pull rod by means of calibrated weights. In the worst cases of an approximately 0.4 mm thick specimen, a nominal engineering stress of 230 MPa was guaranteed within ± 6 MPa. Creep tests were carried out at a temperature of 980 °C.

Creep specimens were fixed in alumina clamps and heated in a radiation furnace in air or under vacuum. Strain was measured with an error of $\Delta\varepsilon \approx \pm 0.07\%$ with a non-contacting video extensometer [21,22], avoiding any grooves on the miniature specimens. Temperature regulation was realized with type-S thermocouples. Table 2 gives an overview of the creep tests carried out.

Table 2. Overview of creep tested specimens. Creep tests with conditions highlighted in bold were carried out twice.

Wall Thickness	In Air			Under Vacuum		
	With Casting Surface	Without Casting Surface	Prepared from Bulk Material	With Casting Surface	Without Casting Surface	Prepared from Bulk Material
0.4 mm	150 MPa	230 MPa	150 MPa	150 MPa	230 MPa	230 MPa
	190 MPa		230 MPa	230 MPa		
	230 MPa					
0.8 mm	150 MPa	230 MPa	230 MPa	150 MPa	230 MPa	230 MPa
	230 MPa			230 MPa		
1.0 mm	230 MPa	230 MPa	230 MPa	230 MPa	230 MPa	230 MPa
2.0 mm	150 MPa	230 MPa	230 MPa	230 MPa	230 MPa	230 MPa
	230 MPa					

Creep tests with 150 MPa, 190 MPa and 230 MPa engineering stress were carried out on selected samples for the determination of the stress exponent n in a power law relation between the minimum creep rate and the engineering stress.

$$\dot{\varepsilon}_{min} = c \cdot \sigma^n \quad (1)$$

2.3. Microstructural Characterization

Microstructural investigations were carried out with a scanning electron microscope (SEM) 1540 EsB Cross Beam (Zeiss, Jena, Germany) operating at 15 kV accelerating voltage. Secondary electron imaging was carried out with an Everhart–Thornley detector. The chemical composition of surface and oxide layers was determined using energy-dispersive X-ray spectroscopy (EDS). Cross and longitudinal sections of each specimen after heat treatment and creep deformation were embedded, ground with SiC paper, polished with diamond slurry and, finally, polished with colloidal silica. Thereafter, the specimens were etched with a solution of 3 g Mo-(VI)-oxide, 100 mL H₂O, 100 mL HNO₃ and 100 mL HCl, preferentially dissolving the γ' phase.

Samples for TEM analysis were prepared using a Scientific SCIOS DualBeam SEM (Thermo Fisher, Waltham, MA, USA) with a Ga ions FIB system. Cross-section specimens were removed with milling trenches using an ion beam accelerating voltage of 30 kV and currents between 30 nA and 300 pA. Thinning of TEM lamellas to <100 nm thickness was carried out using 2 kV ion beam accelerating voltage and 35 pA ion beam current. TEM analysis was conducted with a JEOL 2100Plus (Jeol, Freising, Germany) at 200 kV acceleration voltage. Dark field images to reveal an ordered structure were taken with a $\vec{g} = \langle 001 \rangle$ diffraction vector.

3. Results

3.1. Microstructure

An approximately 3–5 μm thick surface layer was observed after the heat treatment of the thin-cast MAR M247LC under vacuum, see Figure 2a. Beneath this layer, there was a homogeneous matrix/ γ' structure with cuboidal γ' precipitates.

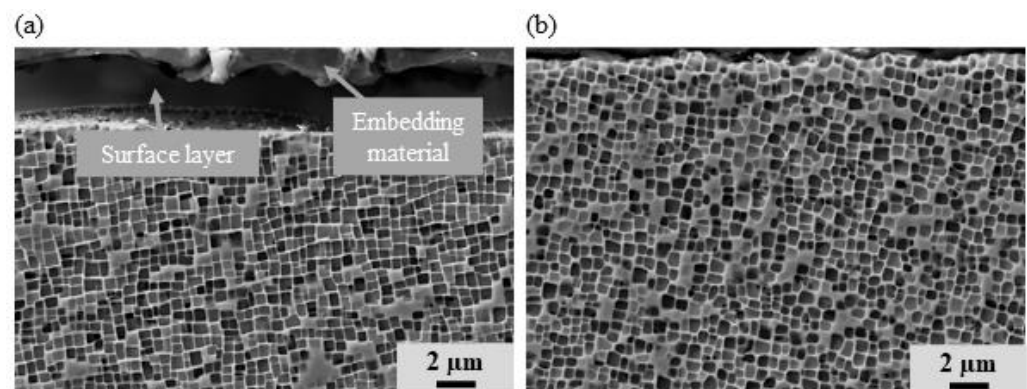


Figure 2. Microstructure in the near-surface area after heat treatment under vacuum of thin-cast specimens (a) with surface layer, (b) surface layer removed by grinding with SiC paper with grits of 1000.

Figure 3 gives the chemical composition of the surface layer. An enrichment of the γ' -forming element aluminum alongside a nickel enrichment was detected, while chromium and cobalt were depleted within this layer.

The surface layer observed after the heat treatment under vacuum was further investigated with TEM. An electron transparent lamella was prepared with the FIB technique described above so that both the single-phase surface layer (area 1 in Figure 3) and the two-phase structure (area 2 in Figure 3) could be analyzed in the TEM (see Figure 4a). Figure 4b illustrates the TEM diffraction patterns within the surface layer and the two-phase structure. Figure 4c shows a TEM dark field diffraction contrast image obtained with superlattice reflection. Here, γ' appears in light shading and the matrix phase in dark. The superlattice diffraction spots of an L1₂ ordered phase together with the chemical composition given in Figure 3 verified that the surface layer was single-phase γ' . Hence, for the so-called creep tests with casting surface, the initial surface at the beginning of the test consisted of single-phase γ' .

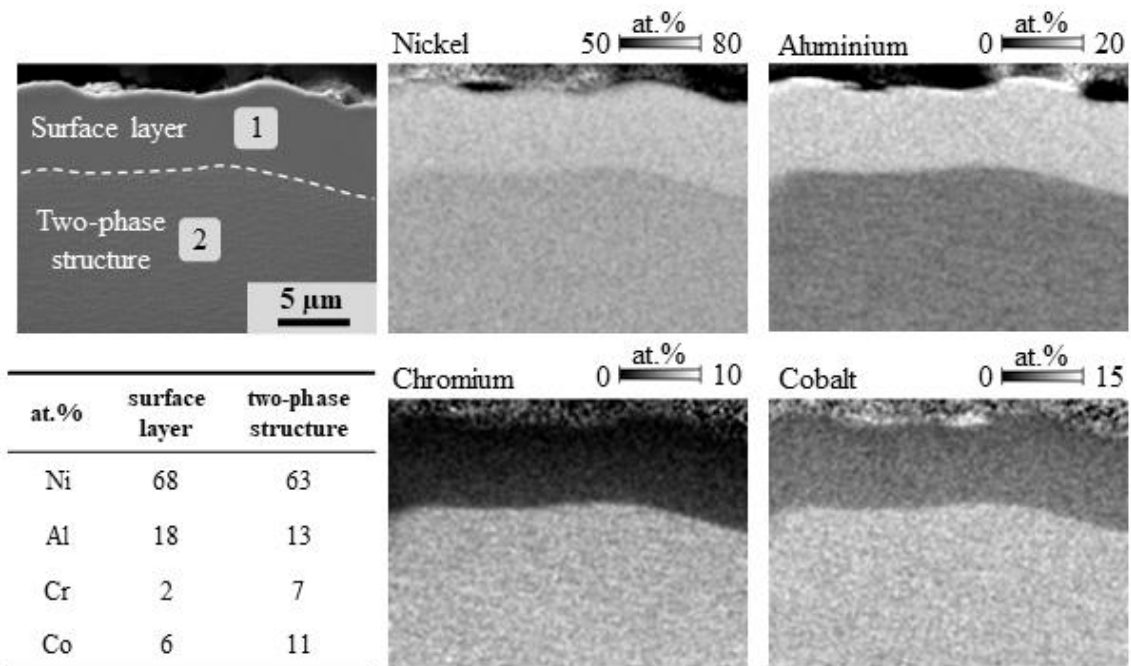


Figure 3. Chemical composition of the surface layer formed during heat treatment under vacuum.

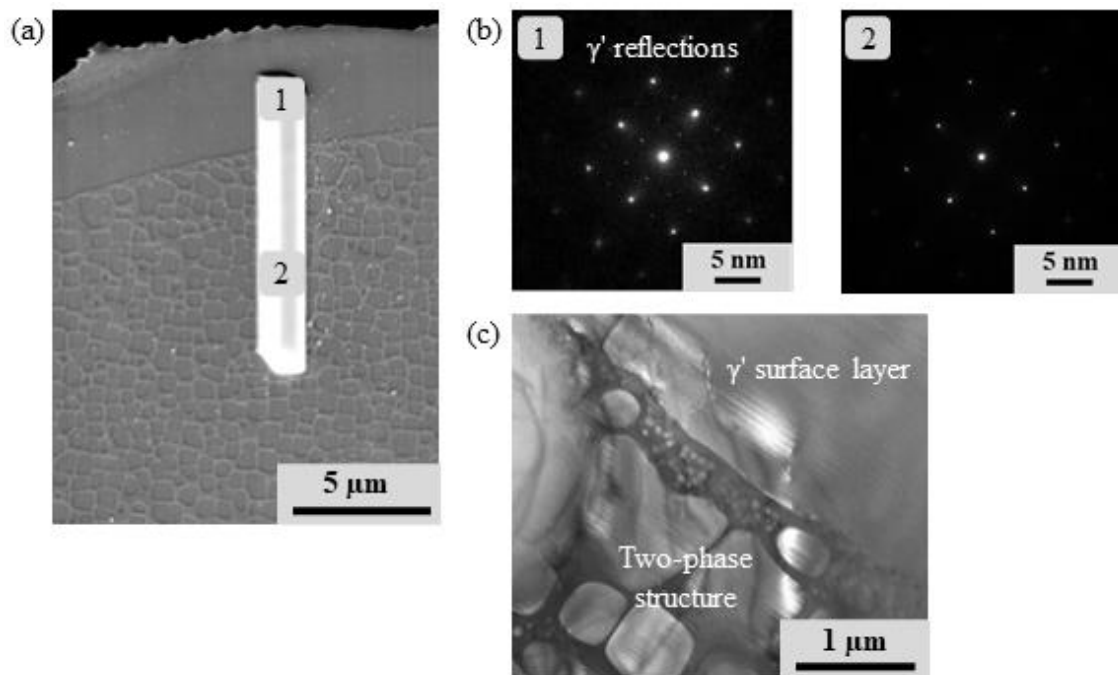


Figure 4. TEM lamella preparation and TEM analysis: (a) position of TEM lamella prepared with focused ion beam; (b) TEM diffraction patterns in the surface layer (area 1) and the two-phase structure; (c) dark field image with γ' reflection of the transition area.

Surface grinding for the so-called creep tests without casting surface removed the single-phase γ' -scale, so that the homogeneous matrix/ γ' structure reached up to the creep specimen surface (see Figure 2b).

Figure 5 shows typical SEM images of near surface areas of single-crystal MAR M247LC after creep deformation in air (Figure 5a) and under vacuum (Figure 5b). During creep deformation in air, a γ' -free zone was formed beneath an oxide layer. Below these two zones, a rafted two-phase structure was seen (Figure 5a). In contrast, creep tests under

vacuum prevented oxidation and a γ' -free zone was not detected. The rafted microstructure was present up to the specimen surface. In both cases, rafting of the γ' precipitates took place perpendicular to the load direction, anticipated for a nickel-based superalloy with a negative misfit under tensile load [23,24]. The bright areas correspond to the matrix, whereas the darker areas are γ' phase.

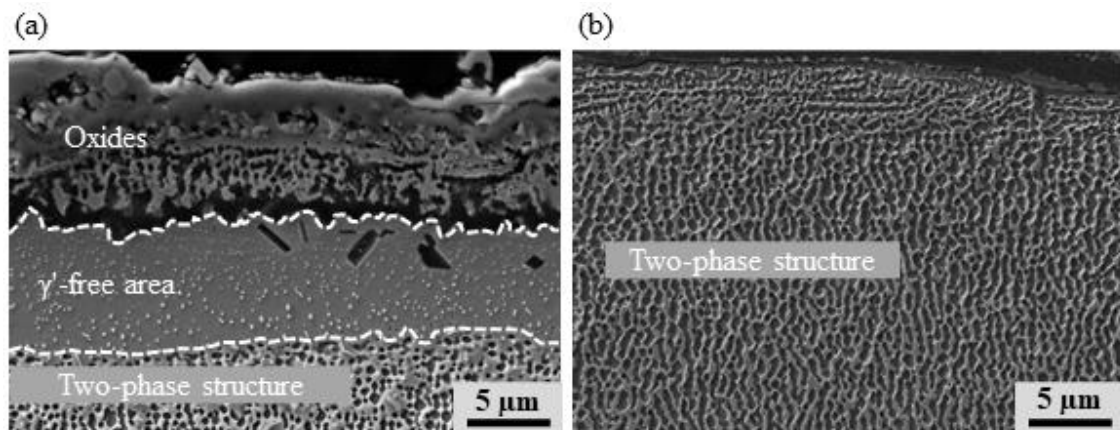


Figure 5. Microstructure after creep deformation at 980 °C and 230 MPa (a) in air after 50 h and (b) under vacuum after 75 h.

3.2. Creep Behavior

Figure 6 shows the strain versus time and strain rate versus strain creep curves of the single-crystal MAR M247LC specimens with various thicknesses in air at 980 °C and under an engineering tensile stress of 230 MPa. Rupture of the specimens was marked in the diagrams with a cross. Creep diagrams were divided according to three different surface conditions, i.e., with casting surface (Figure 6a,b), without casting surface (Figure 6c,d) and prepared from bulk material (Figure 6e,f).

The rupture times of all the creep tests carried out in air at 230 MPa and 980 °C, independent from the thickness, were in the same range, i.e., in between 40 and 75 h. Except for one outlier with a 0.4 mm thickness, the strains at rupture were in a single range of 20–25%. In addition, the creep curves all showed very similar progressions. A short primary creep was present with decreasing creep rates. Minimum creep rates were generally reached after just 1–2.5% engineering strain. The creep accelerated steadily after minimum creep rates were reached, which could be attributed to microstructural changes due to rafting. No pronounced secondary creep with an approximately constant creep rate was observed, but rather, a tertiary creep started immediately after the primary creep.

Figure 7 shows the creep curves of specimens with casting surface of different wall thicknesses tested in air at 980 °C under an engineering stress of 150 MPa. A creep rupture for wall thicknesses of 0.4 and 0.8 mm took place after 200 h. These two creep curves showed sharp increases in the creep rate near the ends of their live times, hence, very much different progressions than all creep curves from tests under 230 MPa at 980 °C in air. The creep test of the specimen with a wall thickness of 2 mm was interrupted after approximately 180 h, because an almost constant creep rate was reached.

Figure 8 shows the creep curves of tests under vacuum at 980 °C and an engineering stress of 230 MPa again carried out on specimens with various thicknesses and surface conditions. With the single exception of a 2 mm thick specimen prepared from the bulk, the rupture times of all the creep tests carried out in vacuum at 230 MPa and 980 °C were in the same range of 25–100 h. Strains at rupture in all creep tests were also in a single range of 25–30%. All creep curves showed very similar progressions reaching minimum creep rates after 1–2.5% engineering strain. Thereafter, creep accelerated steadily, typical for tertiary creep.

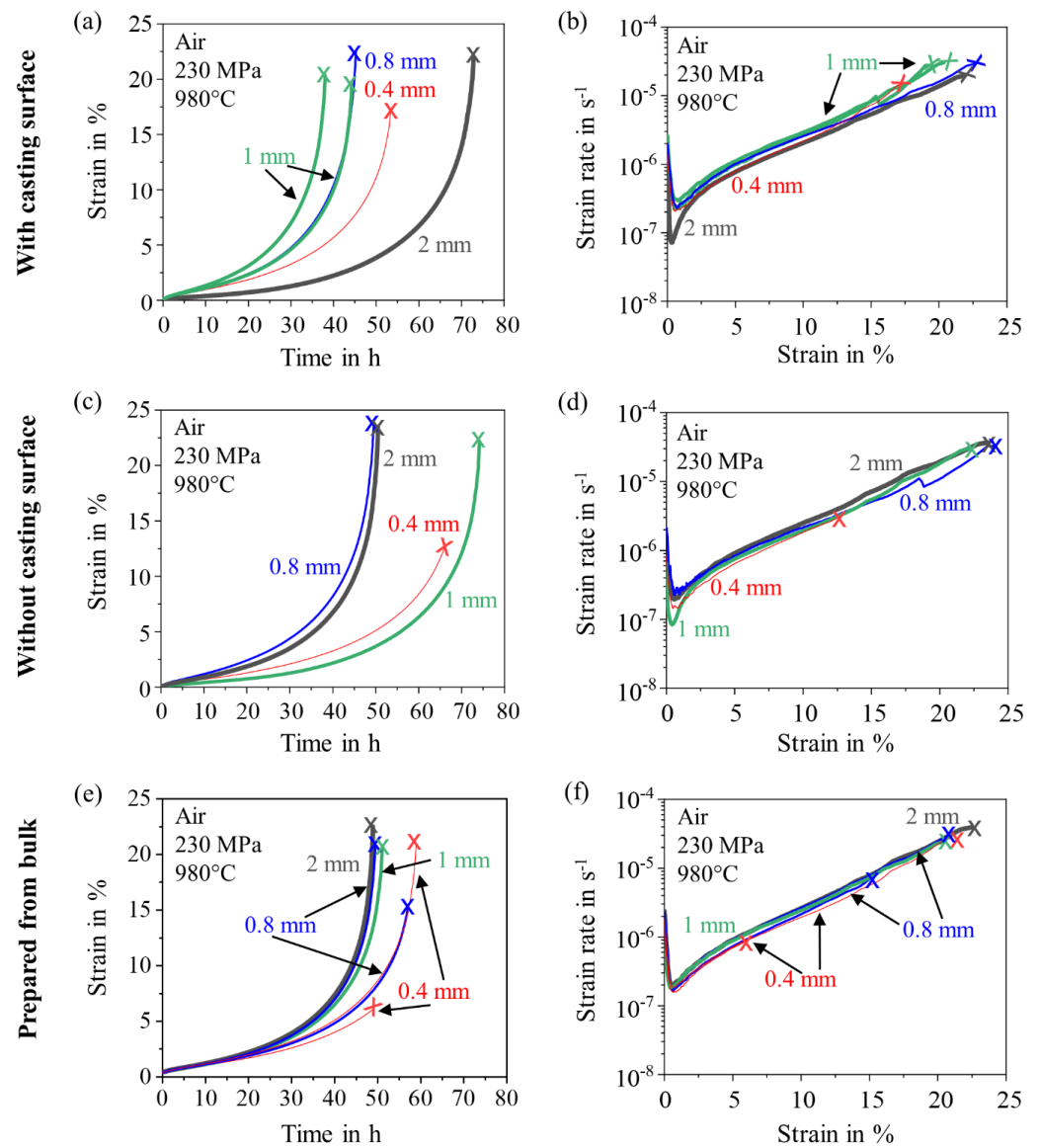


Figure 6. Creep curves of specimens with various thickness tested in air at 980 °C under a high stress of 230 MPa: (a,b) with casting surface, (c,d) without casting surface, (e,f) prepared from bulk material.

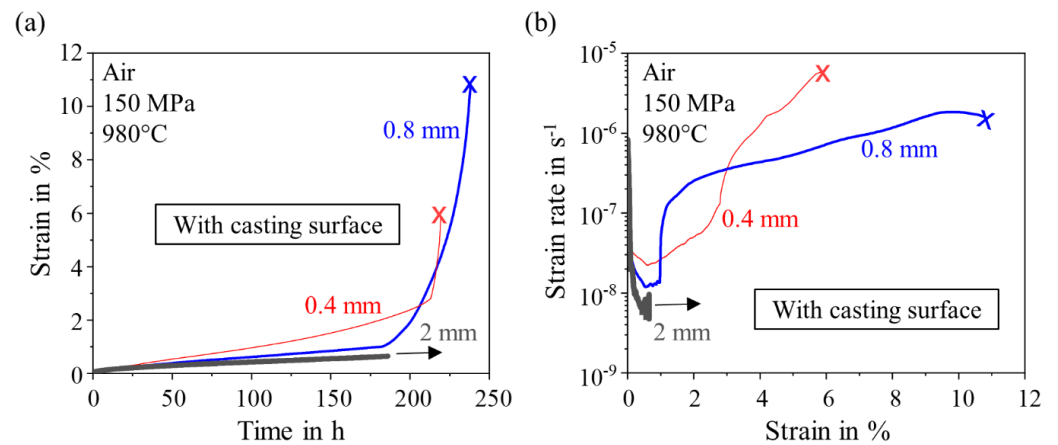


Figure 7. Creep curves of thin-cast specimens with casting surface of different wall thickness in air at 980 °C under a low stress of 150 MPa: (a) strain versus time; (b) strain rate versus strain.

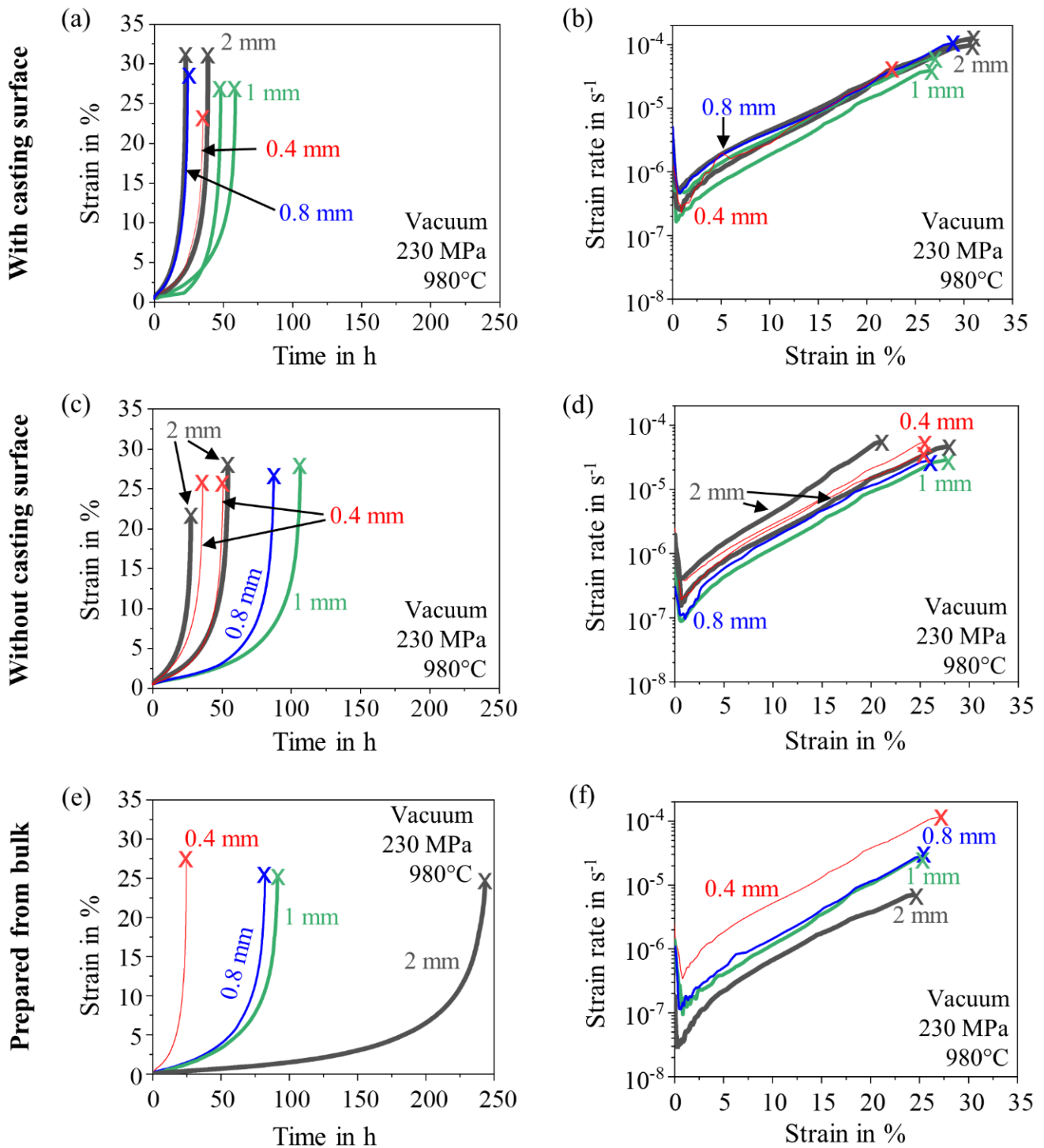


Figure 8. Creep curves of thin-walled specimens for the investigation of the influence of the wall thickness under vacuum at a stress of 230 MPa at 980 °C: (a,b) with casting surface, (c,d) without casting surface, (e,f) prepared from bulk material.

4. Discussion

The formation of a single-phase γ' layer during a heat treatment under vacuum was caused by the high vapor pressures of chromium and cobalt. Chromium and cobalt are elements that stabilize the matrix. If these elements evaporate during a heat treatment, the matrix phase dissolves and the γ' phase becomes stabilized [25–27].

The stress exponent in the power law relation between the minimum creep rate and the engineering stress of the single-crystal MAR M247LC in the [001] orientation was in the range of 5–7 in all circumstances. Hence, it was independent from the surface condition, the specimen thickness and the creep test atmosphere. It may be concluded that the dominant creep deformation mechanism was a dislocation climb [23] in all circumstances. Stress exponents in this work at a temperature of 980 °C were in good agreement with the literature, which indicated a stress exponent of 8.4 in creep tests under vacuum with stresses of 150 MPa and 230 MPa [17]. Bensch et al. [13] examined the stress exponent n of the single-crystal nickel-based superalloy MAR M247LC at 980 °C too. The stress exponent was expected to be 5.6 with a γ' volume fraction of 49%, while it was 8.7 with a γ' volume fraction of 62%.

Cast nickel-based superalloy MAR M247LC single crystals with various thickness were creep tested at 980 °C in air and vacuum and in two distinct load regimes, i.e., under a high engineering load of 230 MPa and a low engineering load of 150 MPa. Different surface conditions (with or without casting surface, prepared from bulk), tested both in air and under vacuum, showed that specimen surface conditions do not play a major role. Previous investigations on thin-cast polycrystalline specimens of the nickel-based superalloy IN100 with wall thicknesses of 0.9 and 1.3 mm confirmed this observation [28].

In addition, at high engineering loads, leading to generally short creep live times, creep properties turned out to be independent from the wall thickness. The scatter of the creep live times was within the usual deviation for creep experiments [29]. In contrast, at the low engineering load level and, therefore, longer creep live times (>200 h), a clear thickness debit effect was observed.

In the literature it is commonly observed that the thickness debit effect is more pronounced at higher temperatures and lower stress levels, i.e., longer creep times. Krieg et al. [16] observed a significant reduction in creep life with decreasing wall thickness (0.3/0.5/1.0 mm) on thin-walled specimens of the nickel-based superalloy PWA 1484 prepared from bulk single crystals (70/80 MPa, 1100 °C). In contrast to that, no significant thickness debit effect was detected for 170 MPa at 980 °C [16].

Brunner et al. [17] illustrated a corresponding behavior in thin specimens prepared from bulk material with a wall thickness of 0.3 and 1 mm of the single-crystal nickel-based superalloy MAR M247LC. At a low stress level (150 MPa, 980 °C) or at higher temperatures (i.e., 1100 °C), creep strength decreases more with decreasing wall thickness compared to higher stress levels (230 MPa, 980 °C) [17].

Bensch et al. [11,30] identified oxide layer formation and the associated growth of γ' -free and γ' -depleted areas as a decisive factor influencing the creep behavior of thin-walled specimens of nickel-based superalloys. Bensch et al. [11,30] demonstrated experimentally and with model simulations that the strength of the thickness debit effect also depends on the chemical composition of a single-crystal nickel-based superalloy. Simulations estimated that creep properties of MAR M247LC deteriorate by 50% as soon as the wall thickness is inferior by 0.4 mm. The determined critical wall thickness for René N5 was approximately 0.6 mm. Compared to MAR M247LC, René N5 showed a more pronounced thickness debit effect due to a stronger Al_2O_3 layer formation [11,30]. This also corresponded to experimental investigations of Hüttner et al. [14,15] regarding the thickness debit effect in the single-crystal nickel-based superalloy René N5. Figure 9 summarizes the rupture times or creep live times, respectively, as a function of the wall thickness of the single-crystal nickel-based superalloys MAR M247LC and René N5.

The thickness debit effect was obviously governed by diffusion-controlled mechanisms. The formation of oxide layers and γ' -free/depleted areas played the decisive role. Hence, the thickness debit effect itself was notably time dependent. If creep deformation lasted long enough (>200 h, 980 °C), a significant proportion of the cross-sectional area was affected by these diffusion-controlled mechanisms, leading to deteriorating creep properties.

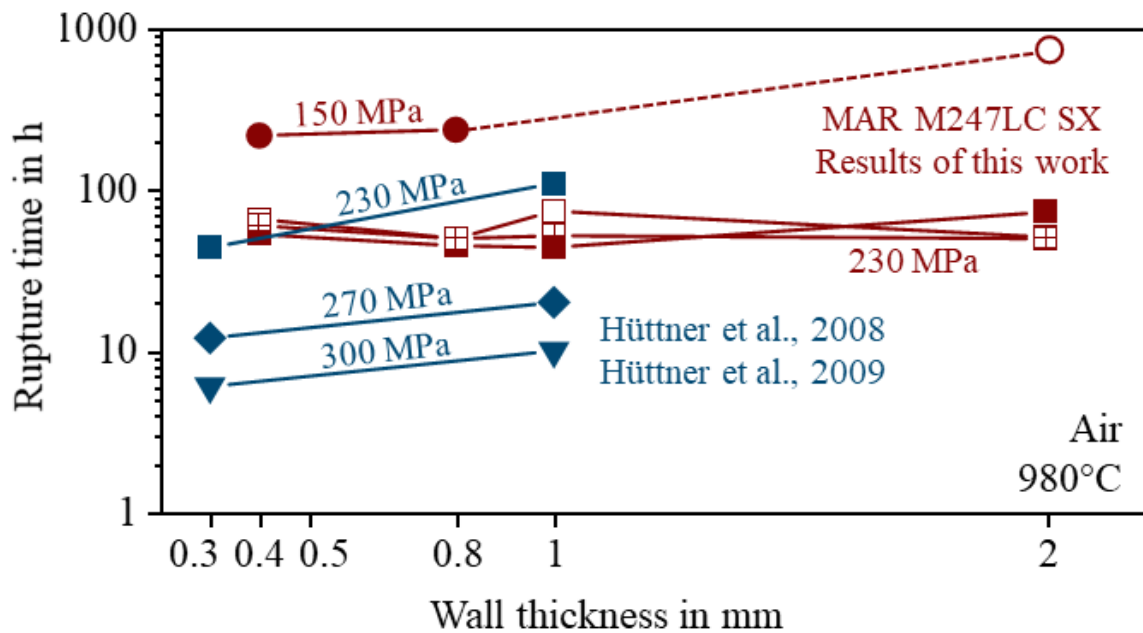


Figure 9. Summary of the results of this work in comparison to literature: rupture time over wall thickness at 980 °C in air; Data from [14,15].

5. Conclusions

Creep tests at 980 °C on thin nickel-based superalloy MAR M247LC single crystals were carried out in air and under vacuum. The influence of the surface condition and wall thickness (0.4/0.8/1.0/2.0 mm) on the creep behavior was investigated.

- Heat treatment under vacuum at an ambient pressure of 10^{-4} Pa led to a single-phase γ' surface layer.
- Surface condition did not affect the creep behavior of thin specimens.
- Creep tests at 980 °C under 230 MPa leading to creep rupture times <100 h showed no significant thickness debit effect.
- Creep tests at 980 °C under 150 MPa, leading to significantly longer creep rupture times (>200 h), showed a significant thickness debit effect, i.e., a strong deterioration of creep properties with wall thicknesses of 0.8–0.4 mm.
- Thickness debit effect was time-dependent, i.e., it was governed by the formation of oxide layers and γ' -free or γ' -depleted areas. With increasing creep times, these diffusion-controlled mechanisms affected larger proportions of the cross-section, thus, deteriorating the creep properties.

Author Contributions: Conceptualization, S.K., U.G. and R.V.; methodology, S.K.; software, S.K. and R.V.; validation, S.K.; formal analysis, S.K.; investigation, S.K. and S.W.-G.; resources, S.K.; data curation, S.K. and S.W.-G.; writing—original draft preparation, S.K.; writing—review and editing, U.G. and R.V.; visualization, S.K.; supervision, U.G.; project administration, U.G. and R.V.; funding acquisition, U.G. All authors have read and agreed to the published version of the manuscript.

Funding: This research was funded by Deutsche Forschungsgemeinschaft (DFG), research project number GL 181/52-1.

Institutional Review Board Statement: Not applicable.

Informed Consent Statement: Not applicable.

Data Availability Statement: Not applicable.

Conflicts of Interest: The authors declare no conflict of interest.

References

1. Gibbons, T.B. The performance of Superalloys. *Adv. Mater.* **1990**, *2*, 583–588. [\[CrossRef\]](#)
2. Duhal, D.N. Directionally Solidified Superalloys. In *Superalloys II*; Sims, C.T., Stoloff, N.S., Hagel, W.S., Eds.; John Wiley & Sons, Inc.: New York, NY, USA; Chichester, UK; Brisbane, Australia; Toronto, ON, Canada; Singapore, 1987; pp. 189–214.
3. Doner, M.; Heckler, J.A. Identification of Mechanisms Responsible for Degredation in Thin-Wall Stress-Rupture Properties. *Proc. Int. Symp. Superalloy.* **1988**, 653–662. [\[CrossRef\]](#)
4. Baldan, A. Combined effects of thin-section size, grain size and cavities on the high temperature creep fracture properties of a nickel-base superalloy. *J. Mater. Sci.* **1997**, *32*, 35–45. [\[CrossRef\]](#)
5. Gibbons, T.B. Creep properties of Nimonic 90 in thin section. *Met. Technol.* **1981**, *8*, 472–475. [\[CrossRef\]](#)
6. Doner, M.; Heckler, J.A. Effects of Section Thickness and Orientation on Creep-Rupture Properties of Two Advanced Single Crystal Alloys. *SAE Tech. Pap.* **1985**, 851785. [\[CrossRef\]](#)
7. Baldan, A. On the thin-section size dependent creep strength of a single crystal nickel-base superalloy. *J. Mater. Sci.* **1995**, *30*, 6288–6298. [\[CrossRef\]](#)
8. Pandey, M.C.; Taplin, D.M.R. Prediction of rupture lifetime in thin sections of a nickel base superalloy. *Scr. Metall. Mater.* **1994**, *31*, 719–722. [\[CrossRef\]](#)
9. Pandey, M.C.; Taplin, D.M.R.; Rao, P.R. An analysis of specimen geometry effect on the creep life of inconel alloy X-750. *Mater. Sci. Eng. A* **1989**, *118*, 33–39. [\[CrossRef\]](#)
10. Seetharaman, V.; Cetel, A.D. Thickness debit in creep properties of PWA 1484. *Proc. Int. Symp. Superalloy.* **2004**, 207–214. [\[CrossRef\]](#)
11. Bensch, M.; Preußner, J.; Hüttner, R.; Obigodi, G.; Virtanen, S.; Gabel, J.; Glatzel, U. Modelling and analysis of the oxidation influence on creep behaviour of thin-walled structures of the single-crystal nickel-base superalloy René N5 at 980 °C. *Acta Mater.* **2010**, *58*, 1607–1617. [\[CrossRef\]](#)
12. Srivastava, A.; Gopagoni, S.; Needleman, A.; Seetharaman, V.; Staroselsky, A.; Banerjee, R. Effect of specimen thickness on the creep response of a Ni-based single-crystal superalloy. *Acta Mater.* **2012**, *60*, 5697–5711. [\[CrossRef\]](#)
13. Bensch, M.; Fleischmann, E.; Konrad, C.H.; Fried, M.; Rae, C.M.F.; Glatzel, U. Secondary Creep of Thin-Walled Specimens Affected by Oxidation. *Proc. Int. Symp. Superalloy.* **2012**, 387–394. [\[CrossRef\]](#)
14. Hüttner, R.; Gabel, J.; Glatzel, U.; Völkl, R. First creep results on thin-walled single-crystal superalloys. *Mater. Sci. Eng. A* **2009**, *510–511*, 307–311. [\[CrossRef\]](#)
15. Hüttner, R.; Völkl, R.; Gabel, J.; Glatzel, U. Creep behavior of thick and thin walled structures of a single crystal nickel-base superalloy at high temperatures—Experimental method and results. *Proc. Int. Symp. Superalloy.* **2008**, 719–724. [\[CrossRef\]](#)
16. Krieg, F.; Mosbacher, M.; Fried, M.; Affeldt, E.; Glatzel, U. Creep and Oxidation Behaviour of Coated and Uncoated Thin Walled Single Crystal Samples of the Alloy PWA1484. *Proc. Int. Symp. Superalloy.* **2016**, 773–779. [\[CrossRef\]](#)
17. Brunner, M.; Bensch, M.; Völkl, R.; Affeldt, E.; Glatzel, U. Thickness influence on creep properties for Ni-based superalloy M247LC SX. *Mater. Sci. Eng. A* **2012**, *550*, 254–262. [\[CrossRef\]](#)
18. Konrad, C.H.; Brunner, M.; Kyrgyzbaev, K.; Völkl, R.; Glatzel, U. Determination of heat transfer coefficient and ceramic mold material parameters for alloy IN738LC investment castings. *J. Mater. Process. Technol.* **2011**, *211*, 181–186. [\[CrossRef\]](#)
19. Körber, S.; Völkl, R.; Glatzel, U. 3D printed polymer positive models for the investment casting of extremely thin-walled single crystals. *J. Mater. Process. Technol.* **2021**, *293*, 117095. [\[CrossRef\]](#)
20. Körber, S.; Fleck, M.; Völkl, R.; Glatzel, U. Anisotropic Growth of the Primary Dendrite Arms in a Single-Crystal Thin-Walled Nickel-Based Superalloy. *Adv. Eng. Mater.* **2022**, *24*, 2101332. [\[CrossRef\]](#)
21. Völkl, R.; Freund, D.; Fischer, B. Economical Creep Testing of Ultrahigh-temperature Alloys. *J. Test. Eval* **2003**, *31*, 35–43.
22. Völkl, R.; Fischer, B. Mechanical Testing of Ultra-high Temperature Alloys. *Exp. Mech.* **2004**, *44*, 121–128. [\[CrossRef\]](#)
23. Kassner, M.E. *Fundamentals of Creep in Metals and Alloys*; Elsevier: Amsterdam, The Netherlands, 2008. [\[CrossRef\]](#)
24. Epishin, A.; Link, T.; Portella, P.D.; Brückner, U. Evolution of the γ/γ' microstructure during high-temperature creep of a nickel-base superalloy. *Acta Mater.* **2000**, *48*, 4169–4177. [\[CrossRef\]](#)
25. Schulze, M.; Seidel, S. *Verdampfungs-gleichgewicht und Dampfdruck*; Springer Fachmedien: Wiesbaden, Germany, 2018. [\[CrossRef\]](#)
26. Alcock, C.B.; Itkin, V.P.; Horrigan, M.K. Vapour pressure equations for the metallic elements: 298–2500K. *Can. Metall. Q.* **1984**, *23*, 309–313. [\[CrossRef\]](#)
27. D'Souza, N.; Welton, D.; Kelleher, J.; West, G.D.; Dong, Z.H.; Brewster, G.; Dong, H.B. Microstructure instability of ni-base single crystal superalloys during solution heat treatment. *Proc. Int. Symp. Superalloy.* **2016**, 267–277. [\[CrossRef\]](#)
28. Strößner, J.; Konrad, C.H.; Brunner, M.; Völkl, R.; Glatzel, U. Influence of casting surface on creep behaviour of thin-wall Ni-base superalloy Inconel100. *J. Mater. Process. Technol.* **2013**, *213*, 722–727. [\[CrossRef\]](#)
29. Evans, R.W.; Wilshire, B. *Creep of Metals and Alloys*; U.S. Department of Energy: Oak Ridge, TN, USA, 1985; ISBN 0904357597.
30. Bensch, M.; Sato, A.; Warnken, N.; Affeldt, E.; Reed, R.C.; Glatzel, U. Modelling of High Temperature Oxidation of Alumina-Forming Single-Crystal Nickel-Base Superalloys. *Acta Mater.* **2012**, *60*, 5468–5480. [\[CrossRef\]](#)